Lecture Notes in Electrical Engineering 1052

Bálint Németh *Editor*

Proceedings of the 16th International Conference on Electrostatic Precipitation

Springer

Editor
Bálint Németh
Head of High Voltage Laboratory
Budapest University of Technology and Economics
Budapest, Hungary

ISSN 1876-1100 ISSN 1876-1119 (electronic)
Lecture Notes in Electrical Engineering
ISBN 978-3-031-34525-8 ISBN 978-3-031-34526-5 (eBook)
https://doi.org/10.1007/978-3-031-34526-5

This Springer imprint is published by the registered company Springer Nature Switzerland AG
The registered company address is: Gewerbestrasse 11, 6330 Cham, Switzerland

Influence of Electrode System Geometry on Efficiency of Particle Collection of a Compact Electrostatic Precipitator for Small Scale Biomass Combustion

Andrei Bologa[1](✉) and Hans P. Rheinheimer[2]

[1] Karlsruhe Institute of Technology, Institute for Technical Chemistry, 76344 Eggenstein-Leopoldshafen, Germany
andrei.bologa@kit.edu
[2] CCA-Carola Clean Air GmbH, 76344 Eggenstein-Leopoldshafen, Germany
rheinheimer@carola-clean-air.com

Abstract. In the study, attention is given to the development of a compact electrostatic precipitator (ESP) for small-scale biomass combustion facilities. A pilot ESP was tested, being installed downstream the wood-chips and wood-pellets boilers and the wood-logs stove. A DC negative corona discharge was used for particle charging. The ESP was operated at corona voltages up to 22,1 kV and corona currents up to 2,1 mA. The ESP included a casing with gas input and output sections and a grounded removable ash-box installed at a casing bottom part. The ESP with elongated barbed HV electrodes, installed axially inside the gas input section, was characterised with low corona discharge power consumption and reduced particle mass collection efficiency. The next generation electrode systems were tested which included disk and quadrat form barbed HV electrodes, installed inside the ash box, which was used as an opposite electrode. The optimization of HV electrode system geometry enhanced the long-term operation stability of the ESP, ensuring mean mass collection efficiency of 75%.

Keyword: Wood combustion · Fine particle emissions · Electrostatic precipitator · Electrode system geometry · Collection efficiency

1 Introduction

The use of electrostatic precipitators is an effective way for reduction of fine particle emissions from exhaust gases from biomass combustion facilities [1, 2]. The operation of an ESP bases on particle electrostatic charging and precipitation in the corona discharge field [3, 4]. For particle charging in the exhaust gas from biomass combustion units, a direct current (DC) negative polarity corona discharge is preferably applied. At the same value of applied voltage, a DC negative corona discharge allows the generation of corona currents, higher than the DC positive corona. It also shows higher operation stability in hot gas conditions.

B. Németh (Ed.): ICESP 2022, LNEE 1052, pp. 1–14, 2023.
https://doi.org/10.1007/978-3-031-34526-5_1

In the conventional ESPs, the charging and precipitation of particles takes place in the same electrode system (ES) [5, 6]. The ES constellation assumes the use of wire, rod, barbed or lamellar HV electrodes installed between the grounded plates. The HV electrodes could be also installed axially inside the grounded tube casing [3, 7, 8]. The ES of the conventional ESPs, usually, is characterized with large electrode gaps, what demands the application of powerful high voltage units [9]. Large size, automatic cleaning procedures, necessity of external control unit and high maintenance costs often limit the application of conventional ESPs for exhaust gas cleaning from small scale biomass facilities with heat capacity up 100 kW, which are mainly used in the private household for heating purposes [10–13].

The technical solution of the problem of reduction of particulate emissions from small-scale biomass combustion supposes the development of compact ESPs, which are designed to be operated at reduced corona discharge power consumption, assuming manual or automatic cleaning of collected fly ash [2, 13]. These ESPs are preferably designed to be installed between the combustion facility and the chimney. The ESP with automatic cleaning system could be integrated into the combustion facility too.

The design of compact ESPs with manual cleaning is rather simple, what allows considerable reduction of ESPs maintenance and operation costs. However, the loading of ESP electrode system with fly ash remains a technical challenge. The protection of HV insulators against the loading with fly ash and gloss soot is another problem which needs to be solved.

The scope of the current study is the development of a compact ESP for small scale biomass combustion facilities with heat capacity up to 100 kW, which design is realized taking into consideration following demands and conditions: (1) The ESP is designed to be installed between the combustion facility and the chimney. (2) The ESP should be manually cleaned. (3) A DC negative corona discharge is applied for particles charging. (4) ESP needs to ensure high collection efficiency of particles from the exhaust gases during combustion of various types of fuels. (5) The ESP design should ensure long-term operation stability. (6) The cost-effective approach should be applied for reduction of the ESP maintenance and operational costs.

2 Design of Electrostatic Precipitator

The deigned ESP includes a casing with two T-form tubes, fixed between the upper and bottom plates (Fig. 1). An ash-box is installed at the bottom of the casing, and it is designed to be replaceable. The ESP casing and the ash box are grounded and not thermo-insulated. The HV part of the ESP includes an insulator, installed above the casing gas input section. A HV rod penetrates through the HV insulator. It is connected with its upper edge with high voltage power supply unit. The HV lamellar barbed electrodes are installed on the HV rod, ensuring the generation of corona discharge inside the gas input tube section (Fig. 1,a).

The design of the ESP allows the maintenance of two HV insulators with corona discharge electrodes, installed inside the ash box (Fig. 1,b).

In another constellation, the HV electrode system includes single HV insulator, installed above the gas input section, and a HV rod, and plate barbed HV electrodes,

maintained inside the ash box (Fig. 1,c). The barbed electrodes are connected with a HV support.

The ESP is equipped with a HV power supply unit and a temperature sensor, which is installed on the lateral surface of the ESP casing. The signal from the temperature sensor is used to switch on/off the generation of high voltage in dependence of ESP operation conditions.

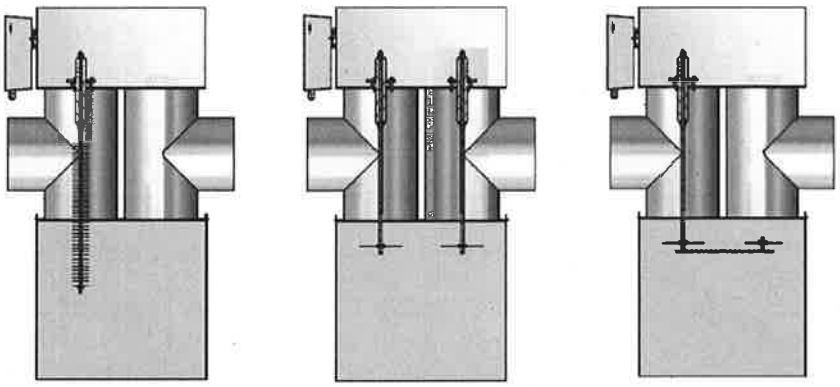

Fig. 1. Compact electrostatic precipitator with various HV electrode systems: (a) single HV insulator, HV rod with lamellar barbed electrode; (b) two HV insulators, two HV rods with plate barbed electrodes inside the ash box; (c) single HV insulator, HV rod and plate barbed electrodes inside the ash box, connected with a HV support

The designed ESP operates in the following way. Particle loaded exhaust gas flows into the ESP through the gas input section. Then gas flows through the ash box and exits from the ESP via the gas output section. When a HV is applied, a DC corona discharge is generated on the sharp points of HV electrodes. In the ESP with lamellar electrode (Fig. 1,a), particle charging takes place inside the gas input section. The precipitation of charged particles takes place due to electrohydrodynamic phenomena in the gas input section, and due to gasdynamic, thermophoretic, and space charge phenomena inside the ash box and gas output section. The electrostatic agglomeration of particles takes place inside the gas input section and the ash box.

In another ESP constellation (Fig. 1,b and Fig. 1,c), particle charging takes place in the corona discharge field, generated between the barbed electrodes and the lateral wall of the ash box, and the bottom plate of ESP casing. The electrostatic agglomeration of particle takes place preferably inside the ash box.

For experimental study, two pilot electrostatic precipitators (ESP-S and ESP-L) were used. The inner diameter of the gas input and output tubes of the ESL-S was 150 mm. The corresponding design elements of the ESP-L had the diameter of 180 mm. The size of the ash box of the ESP-S was L·W·H = 420·200·200 mm. The ash box of ESP-L had the size L·W·H = 420·200·400 mm. The HV rod was connected to the output of a HV power supply unit with maximum power consumption $P_{max} = 60$ W, corona voltage $U_{max} = 22{,}1$ kV, and corona current $I_{max} = 2{,}1$ mA.

3 Test of Pilot ESP with Wood-Chips Boiler

Pilot electrostatic precipitator ESP-L was tested at facility connected to a 100 kW heat capacity wood-chips boiler (Fig. 2). The test facility was equipped with the corresponding periphery, by-pass, control and measurement equipment. During the tests, the following parameters were measured: boiler parameters, exhaust gas velocity in the gas duct; gas composition, gas temperature upstream and downstream the ESP-L; pressure drop in

Fig. 2. ESP-L precipitator at the test facility.

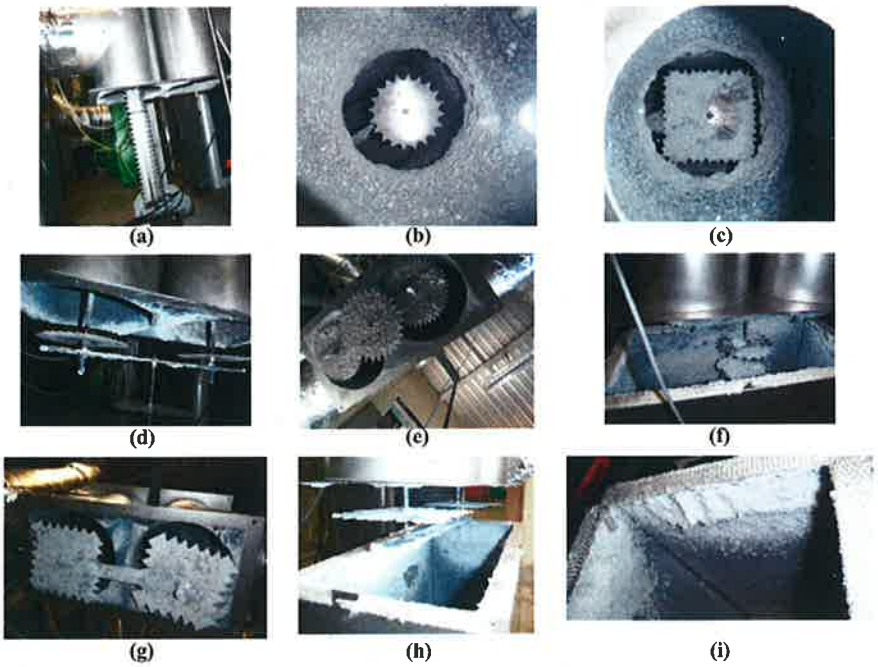

Fig. 3. Electrode systems with variable geometry of high voltage electrodes

the ESP-L; corona discharge voltage U and current I. The data for U and I were used for calculation of corona discharge power consumption P. Particle mass concentrations in the gas flow upstream and downstream the ESP-L were measured simultaneously using analysers type SM 500 (Fa. Wöhler). The data from gravimetric measurements were used for calculation of ESP particle mass collection efficiency.

The ESP-L with various electrode systems (Fig. 3) was studied experimentally. The design of the ESP-L allowed the use of the lamellar barbed electrode, installed axially inside the gas input section (Fig. 3,a). It also allowed the use of disk HV barbed electrodes (Fig. 3,b) or plate quadrat HV barbed electrodes (Fig. 3,c) with variable number of corona discharge sharp points. A part of the lamellar electrode penetrated into the ash box, generating electric field inside the gas input tube and between the HV electrode and the ash box. The HV plate electrodes were installed inside the ash box below the bottom plate and the openings of the gas input and gas output sections (Fig. 3,d and Fig. 3,g). The number of HV electrodes varied from 2 to 4 (Fig. 3,e and Fig. 3,f). It was also varied the position of the electrodes inside the ash box (Fig. 3,g). The HV electrodes were connected with a HV support (Fig. 3,h), which geometry was optimized during the experimental study. The ash box was used as an opposite (grounded) electrode (Fig. 3,j).

The data for corona discharge power consumption and ESP-L mass collection efficiency for various electrode systems (see Table 1) are presented in the Fig. 4. The tests were carried out at gas flow rate of 150 m^3/h. The lamellar HV electrode system ES1 had a large electrode gap, what resulted in reduced electrostatic precipitator mass collection efficiency (Fig. 4). The large length and mass of the lamellar electrode also complicated its adjustment inside the ESP gas input section.

Table 1. Configuration of the electrode system of the electrostatic precipitator.

ES	Electrode system configuration
1	Lamellar barbed electrode in gas input tube
2	3 disk electrodes, Ø 120 mm, 40 mm below bottom plate tube
3	3 disk electrodes, Ø 120 mm, 22 mm below bottom plate
4	3 disk electrodes, Ø 120 mm, 60 mm below bottom plate
5	2 disk electrodes, Ø 120 mm, 60 mm below bottom plate
6	2 disk electrodes, Ø120 mm, 15 mm below bottom plate
7	4 electrodes: 2 disk electrodes, Ø120 mm, 35 mm below bottom plate + 2 electrodes Ø 120 mm, middle position in ash box, 60 mm below separator
8	2 disk electrodes, Ø 120 mm, 35 mm below bottom plate + plus 2 quadrat electrodes 140 mm, middle position in ash box, 60 mm below separator
9	2 electrodes, Ø 120 mm, 25 mm below bottom plate, single HV insulator
10	2 plate electrodes, 140·140 mm, 35 mm below bottom plate
11	2 plate electrodes,140·140 mm, below bottom plate, 1st electrode gap 56 mm, 2nd electrode gap 35 mm

(*continued*)

Table 1. (*continued*)

ES	Electrode system configuration
12	2 plate electrodes, 140·140 mm, 50 mm below bottom plate
13	2 plate electrodes, 140·140 mm, 1st electrode gap 32 mm, 2nd electrode gap 28 mm, below bottom plate
14	2 plate electrodes 140·140 mm, single insulator, 30 mm below bottom plate
15	3 electrodes: 2 plate electrodes 140·140 mm + 1 electrode, Ø 135 mm in the middle of separator, 20 mm below bottom plate
16	3 electrodes: 2 plate electrodes 140·140 mm + 1 electrode, Ø 135 mm in the middle of separator, 40 mm below bottom plate
17	3 electrodes: 2 plate electrodes 140·140 mm + 1 electrode, Ø 135 mm in the middle of separator, 50 mm below bottom plate

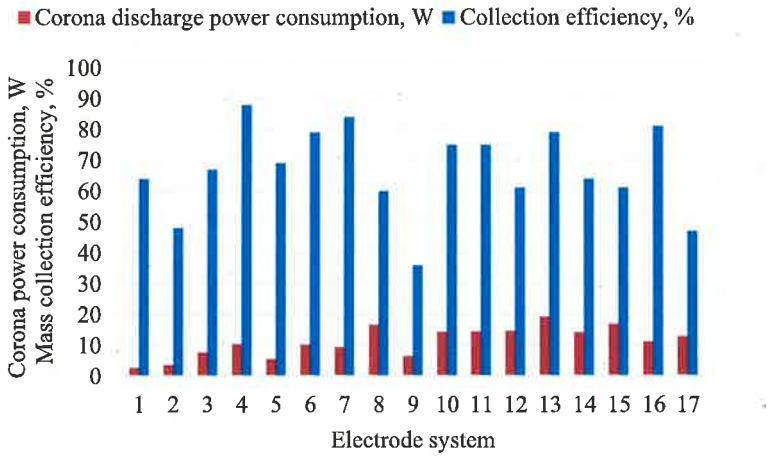

Fig. 4. Corona discharge power consumption and ESP-L mass collection efficiency for various electrode systems, gas flow rate of 150 m^3/h

The next tests were focused on the study of the ESP-L precipitator with disk barbed HV electrodes with diameter of 120 mm (systems ES2-ES9, Table 1). The disk electrodes were installed below the openings of the gas input and output tubes into the ash box. The corona discharge was generated between the HV electrodes sharp points and the opening edges. The tested ES geometry allowed the increase of corona discharge current, but it was sensible to HV electrode adjustment and spark-over discharge voltages. The ESP-L with the configurations ES4, ES6 and ES7 has shown the highest values of mass collection efficiency. The use of the ES7 supposed the maintenance of two supplemental HV electrodes (Fig. 3,f) inside the ash box inner space. These electrodes allowed the generation of an electric field, which enhanced the precipitation of charged particles

inside the ash box. The increase of electrode gap between the HV electrodes and casing bottom plate from 15 mm up to 60 mm resulted in a slight increase of ESP-L mass collection efficiency from 79% to 84%. This effect could be explained by the redistribution of electric field inside the ash box and due to enhancement of charged particles precipitation. Maximum effect was observed with electrode gap width of 60 mm between the HV electrodes and the bottom plate, what corresponded to the width between HV electrodes and the ash box.

The next tests were carried out with quadrat form barbed electrodes with side length of 140 mm (Table 1, systems ES10-ES17). The corona discharge field was generated preferably between the HV electrodes and the lateral wall of the ash box, what increased of corona discharge current and power consumption. Best results were measured for the electrode systems ES10, ES11, ES13 and ES16. The ESP-L with electrode system ES16 had shown the highest mass collection efficiency. The increase of the distance between the casing bottom plate and quadrat barbed electrodes (systems E10, E11 and E13) had only minor influence on the ESP-L mass collection efficiency. In the ES10, two of HV electrodes were used instead of three HV electrodes in the ES16. Hence, the ESP-L collection efficiency with the ES10 was only several percent lower. However, the ES10 system with two electrodes could be easy maintained and adjusted inside the ESP casing.

Taking into consideration the results of the study, the ES10 was recommended to be further used in the ESP-L and ESP-S during the next-coming tests. In the ESPs, the HV quadrate barbed electrodes were installed on the optimized HV support with a distance between HV electrodes and the casing bottom plate of 35 mm.

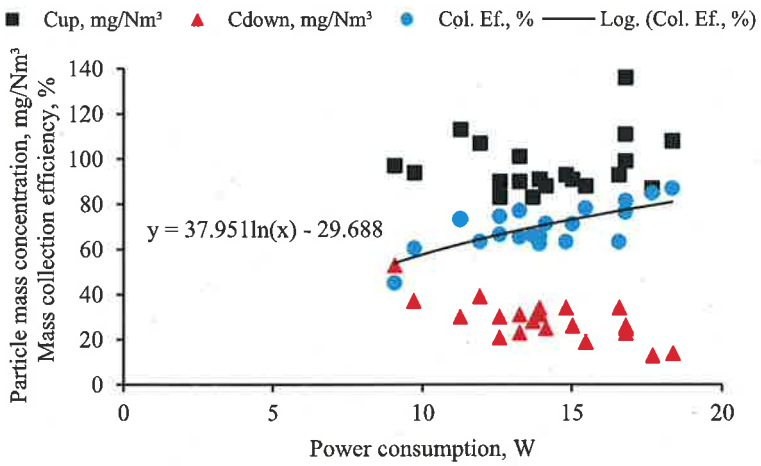

Fig. 5. ESP-L mass collection efficiency in dependence of corona power consumption, gas flow rate of 100 m^3/h, long-term test

The results of the long-term tests of the ESP-L with the ES-10 electrode system are presented in the (Fig. 5), confirming effective particle collection in the designed ESP-L for particle mass concentrations in the exhaust gas 80–140 mg/Nm^3. The experimental

data confirmed the effect of the growing of particle mass collection efficiency with increase of corona discharge power consumption. At constant applied voltage, the change of the gas volume flow from 100 m^3/h up to 150 m^3/h had a minor influence on the mass collection efficiency. The further increase of gas glow rate up to 300 m^3/h resulted in decrease of ESP-L collection efficiency. This took place due to increase of gas velocity inside the ESP, and due to decrease of charged particle precipitation under the influence of space charge phenomena. The growing of gas velocity through the ESP increased the re-entrainment of collected fly ash from the ash box. The increase of gas flow rate also resulted in increase of pressure drop in the precipitator.

4 Test of Pilot ESP with Wood-Pellets Boiler

The pilot ESP-L precipitator was also tested, being installed downstream a wood-pellets boiler with a heat capacity of 12 kW (Fig. 6). The ESP-L was connected with the boiler and the chimney with a 150 mm diameter gas duct. The ESP was operated stop-and-go during four weeks test campaign (total operation time of 90 h). During the tests, the ESP-L was not opened or not cleaned. The gas flow rate through the ESP-L varied between 30–45 m^3/h in dependence of combustion conditions. During stable operation of the boiler, the exhaust gas temperature was 130–135 °C. The ESP-L was operated at corona discharge voltage U = 22,1 kV, current I = 0,6 ± 0,2 mA and power consumption P = 12,5 ± 4,5 W. The results of the measurements are presented in the Fig. 7.

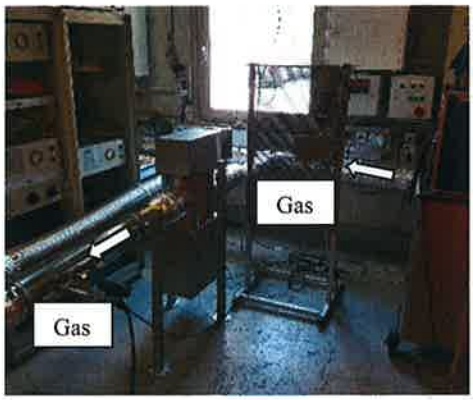

Fig. 6. ESP-L downstream the pellets-boiler

Mean particle mass concentration in the exhaust gas upstream the ESP-L was C_{up} = 15,4 mg/Nm^3 and the downstream the ESP-L it was C_{dowm} = 4,1 mg/Nm^3, what corresponded to particle mass mean collection efficiency of η = 74%. The mean mass collection efficiency remained rather constant during the tests (Fig. 8). The increase of corona discharge power consumption resulted in an enhancement of particle mass collection efficiency.

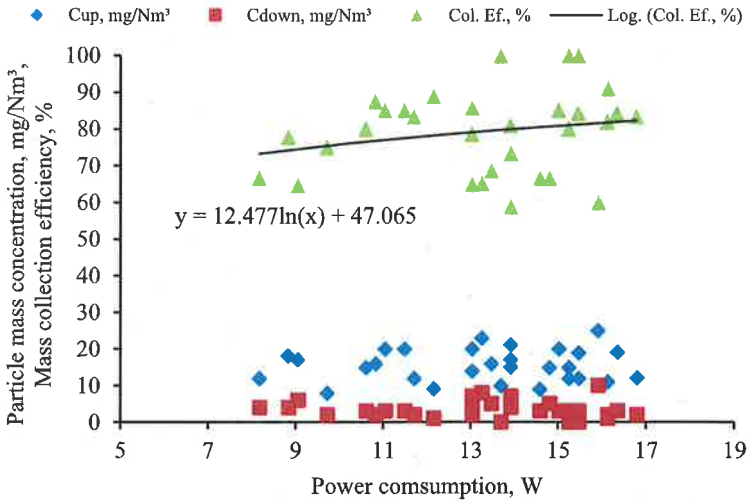

Fig. 7. Particle mass collection efficiency in dependence on corona power consumption

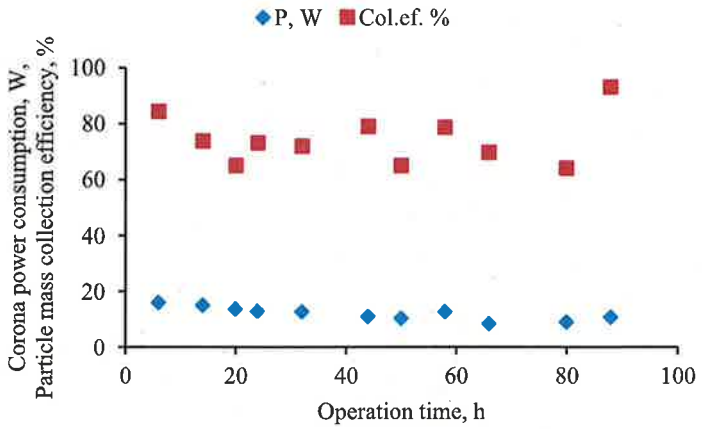

Fig. 8. Corona power consumption and particle mass collection efficiency in due course

5 Test of Pilot ESP with Wood-Logs Stove

The ESP-S was installed downstream a stove with a heat capacity of 9 kW (Fig. 9), being connected with a chimney via the gas duct. The gas duct and ESP-S were not thermo-insulated. During the tests, both wood-logs and coal briquettes were burnt in the stove. The temperature of the exhaust gas varied depending on combustion conditions, reaching its maximum value of 350 °C, mainly after refill of the stove with the fuel. The following parameters were measured during the tests: corona voltage and current, pressure drop in the ESP-S, gas temperature upstream, downstream and inside the ESP-S, gas velocity in the gas duct, particle mass concentrations upstream and downstream the ESP-S. The data for ESP-S mass collection efficiency are presented in the Fig. 10. At U = const,

the increase of particle concentration resulted in corona discharge suppression, and in reduction of corona power consumption (Fig. 11) and ESP-S mass collection efficiency (Fig. 12).

Fig. 9. ESP-S precipitator downstream the stove

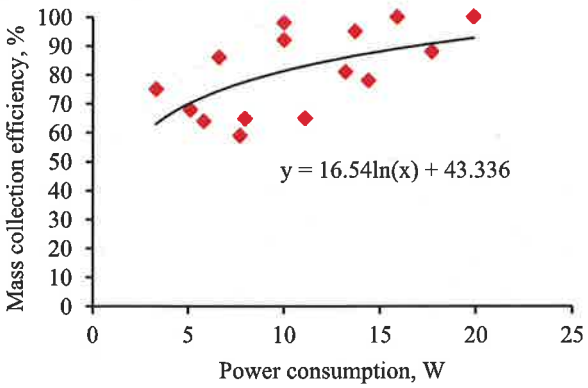

Fig. 10. Dependence of ESP-S mass collection efficiency on corona power consumption

Among the wood-logs, experimental study was carried out with combustion of coal briquettes. During the tests, 50 coal briquettes (every piece of 0,5 kg) were burnt. At the beginning, wood-logs were burnt to heat the stove (Fig. 13, test 1, 6 and 10), and then the briquettes were put into the combustion facility.

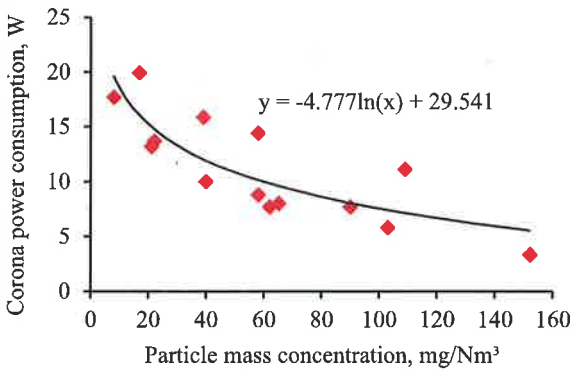

Fig. 11. Dependence of corona power consumption on particle mass concentration in the exhaust gas, wood-logs combustion.

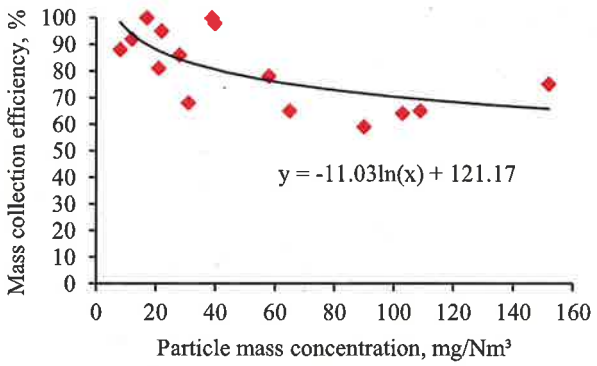

Fig. 12. Dependence of ESP-S mass collection efficiency on particle concentration in the exhaust gas, wood-logs combustion

Every refill of the stove with briquettes was characterized with short-time increase of particle mass concentration downstream the stove: up to 100–150 mg/Nm^3, when a single briquette was put into the stove; up to 500 mg/Nm^3, when 4 briquettes were put into the stove; and up to 1700 mg/Nm^3, when 7 briquettes were simultaneously burnt. The data for the particle mass concentrations are given (Fig. 13) taking into consideration 40% tolerance of the measurement equipment. The coal briquettes "stable combustion" and "post-combustion" phases were characterized with reduced particle mass concentrations in the exhaust gas (Fig. 13, tests 2–5, 7–9 and 11–13). During glowing phase, the reduction of corona discharge suppression was observed, what resulted in the growing of corona discharge current and power consumption and, finally, in increase of the ESP-S particle mass collection efficiency over 90% (Fig. 14, tests 3, 5 and 12).

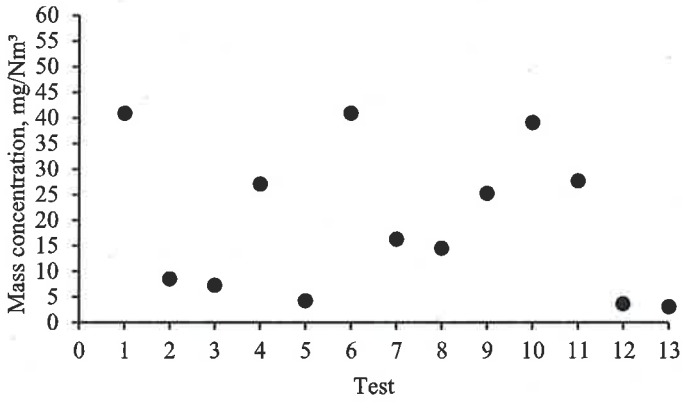

Fig. 13. Particle mass concentration in the exhaust gas, coal briquettes combustion

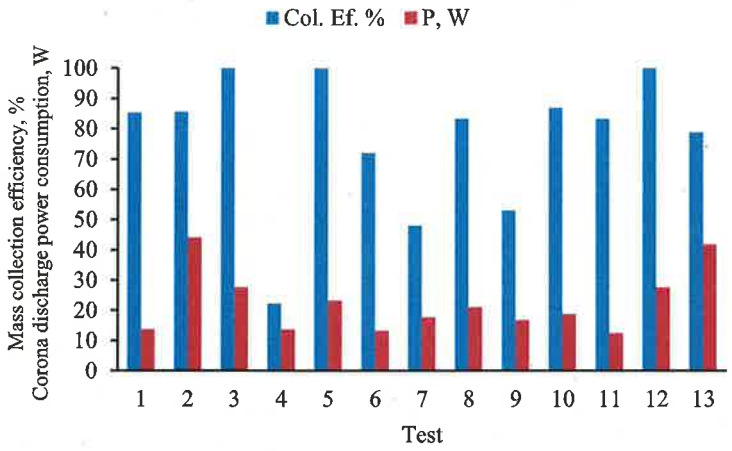

Fig. 14. ESP-S mass collection efficiency and corona power consumption, coal briquettes combustion

6 Conclusions

In the work the results of the development and experimental study of the pilot ESPs are presented and discussed. The compact electrostatic precipitators are designed for reduction of particulate emissions from small scale biomass combustion facilities with the heat capacity up to 100 kW.

Various electrode systems were tested and, finally, an optimized ES configuration was proposed. The ESP constellation included a HV insulator, HV rod and plate barbed HV electrodes installed on a HV support and placed inside the ash box. This electrode configuration allowed the ash box to be used as opposite grounded electrode in the electrode system for generation of corona discharge.

The pilot electrostatic precipitators were tested with wood-chips and wood-pellets boilers, and wood-logs and coal briquettes combustion stove.

The operation of the ESPs is based on the particle electrostatic charging, agglomeration and precipitation. The combined effect of electrohydrodynamic, gasdynamic, thermophoretic, and space charge phenomena, and the use of electrostatic attractive forces between the charged particles and grounded surface of the ESP casing and ash-box allowed to reach the mean particle mass collection efficiency of about 75%.

The optimized design ensured the ESP long-term operation stability for various combustion conditions, temperatures and particle mass concentrations in the exhaust gas.

References

1. Ruttanachot, C., Tirawanichakul, Y., Tekasakul, P.: Application of electrostatic precipitator in collection of smoke aerosol particles from wood combustion. Aerosol Air Qual. Res. **11**, 90–98 (2011). https://doi.org/10.4209/aaqr.2010.08.0068
2. Bologa, A., Paur, H.R., Woletz, K.: Development and study of an electrostatic precipitator for small-scale wood combustion. Int. J. Plasma Environ. Sci. Technol. **5**, 168–173 (2011). https://doi.org/10.34343/ijpest.2011.05.02.168
3. Jaworek, A., Krupa, A., Czech, T.: Modern electrostatic devices and methods for exhaust gas cleaning: a brief review. J. Electrost. **65**, 133–155 (2007). https://doi.org/10.1016/j.elstat.2006.07.012
4. Liao, Z., Li, Y., Xiao, X., Wang, C., Cao, S., Yang, Y.: Electrostatic precipitation of submicron particles with an enhanced unipolar pre-charger. Aerosol Air Qual. Res. **18**, 1141–1147 (2028). https://doi.org/10.4209/aaqr.2017.08.0261
5. Intra, P., Limueadohai, P., Tippayawing, N.: Particulate emissions reduction from biomass burning in small combustion systems with a multiple tubular electrostatic precipitator. Part. Sci. Technol. **28**, 547–565 (2010). https://doi.org/10.1080/02726351003758444
6. Dastoori, K., Kolhe, M., Mallard, C., Makin, B.: Electrostatic precipitation in a small scale wood combustion furnace. J. Electrost. **69**, 466–472 (2011). https://doi.org/10.1016/j.elstat.2011.06.005
7. Trnka, J., Jandačka, J.; Holubčík, M.: Improvement of the standard chimney electrostatic precipitator by dividing the flue gas stream into a larger number of pipes. Appl. Sci. **12**, 2659, 10 p. (2022). https://doi.org/10.3390/app12052659
8. Dastoori, K., Makin, B., Kolhe, M., Des-Roseaus, M., Conneely, M.: CFD modelling of flue gas particulates in a biomass fired stove with electrostatic precipitation. J. Electrost. **71**, 351–356 (2013). https://doi.org/10.1016/j.elstat.2012.12.039
9. Omara, M., Hopke, P.K., Raja, S., Holsen, T.M.: Performance evaluations of a model electrostatic precipitator for an advanced wood combustion system. Energy Fuels **24**, 6501–6306 (2010). https://doi.org/10.1021/ef101031u
10. Oehler, H., Hartmann, H.: Comparative long-term field and test stand measurements at small scale electrostatic precipitators - experiences and measurement strategies. In: 22nd European Biomass Conference and Exhibition, pp. 381–387 (2014). https://doi.org/10.5071/22ndEUBCE2014-2AO.1.4
11. Cid, N., Rico, J.J., Pérez-Orozco, R., Larrañaga, A.: Experimental study of the performance of a laboratory-scale ESP with biomass combustion: discharge electrode disposition, dynamic control unit and aging effect. Sustainability **13**, 10344 (2021). https://doi.org/10.3390/su131810344

12. Brunner, T., Wuercher, G., Obernberger, I.: 2-year field operation monitoring of electrostatic precipitators for residential wood heating systems. Biomass Bioenerg. **111**, 278–287 (2018). https://doi.org/10.1016/j.biombioe.2017.01.025
13. John Carroll, J., Finnan, J.: Use of electrostatic precipitators in small-scale biomass furnaces to reduce particulate emissions from a range of feedstocks. Biosyst Eng. **163**, 94–102 (2017). https://doi.org/10.1016/j.biosystemseng.2017.08.021